Neuron, Vol. 39, 991–1004, September 11, 2003, Copyright ©2003 by Cell Press

Intensity versus Identity Coding in an Olfactory System

Mark Stopfer,[1,2] Vivek Jayaraman,[1] and Gilles Laurent*
California Institute of Technology
Division of Biology
Computation and Neural Systems Program
Pasadena, California 91125

Summary

We examined the encoding and decoding of odor identity and intensity by neurons in the antennal lobe and the mushroom body, first and second relays, respectively, of the locust olfactory system. Increased odor concentration led to changes in the firing patterns of individual antennal lobe projection neurons (PNs), similar to those caused by changes in odor identity, thus potentially confounding representations for identity and concentration. However, when these time-varying responses were examined across many PNs, concentration-specific patterns clustered by identity, resolving the apparent confound. This is because PN ensemble representations changed relatively continuously over a range of concentrations of each odorant. The PNs' targets in the mushroom body—Kenyon cells (KCs)—had sparse identity-specific responses with diverse degrees of concentration invariance. The tuning of KCs to identity and concentration and the patterning of their responses are consistent with piecewise decoding of their PN inputs over oscillation-cycle length epochs.

Introduction

Sensory pathways typically segment objects in the environment into simpler features (e.g., shape, location, motion). Among those, intensity is of great functional importance. Encoding intensity, however, is not a simple matter, for it often interferes with the encoding of other stimulus attributes: in color vision, a photoreceptor's response to dim light at the receptor's optimal wavelength may not differ much from its response to a bright light at a nonoptimal wavelength; this confound can be resolved by population coding using a few broadly tuned and overlapping channels (Rodiek, 1998). We examine here the encoding of odor intensity and its relationship to the encoding of odor identity. We have proposed that, in the olfactory systems of fish and insects, odor identity is encoded by spatiotemporal activity patterns (Friedrich and Laurent, 2001; Laurent, 2002; Laurent et al., 1996; Wehr and Laurent, 1996) across dynamic assemblies of principal neurons (mitral cells, MCs in vertebrates; PNs in insects) in the first olfactory relay (olfactory bulb [OB] or antennal lobe [AL]). Each odor representation can be thought of as a high-dimensional vector of principal neuron states (e.g., instantaneous firing rates) evolving over the duration of the stimulus in a stimulus-specific manner (Laurent et al., 2001). This model, however, has not yet been extended to the context of intensity coding. This is essential, because recordings from amphibians and mammals indicate that MC temporal response patterns change as odor concentration is varied (Kauer and Moulton, 1974; Meredith, 1986; Wellis et al., 1989), raising the possibility that spatiotemporal codes for concentration and identity are confounded. In addition, imaging results indicate that higher odor concentrations increase glomerular response intensity and recruit additional glomeruli (Ng et al., 2002; Wang et al., 2003; Cinelli et al., 1995; Friedrich and Korsching, 1997; Joerges et al., 1997; Meister and Bonhoeffer, 2001; Rubin and Katz, 1999; Stewart et al., 1979), consistent with the observation that MC responses change both quantitatively and qualitatively with odor concentration (Kauer and Moulton, 1974; Meredith, 1986; Wellis et al., 1989). How then are odors represented such that they can be identified over many concentrations, as behavioral experiments in humans, rodents, and insects indicate (Engen and Pfaffmann, 1959; Slotnick and Ptak, 1977; Pelz et al., 1997)? Are there, for example, some invariant features in the responses of principal neurons that allow accurate odor classification across concentrations? We examined this issue in the locust olfactory system by recording the activity of neurons in the AL and of Kenyon cells (KCs), the PNs' targets in the mushroom bodies, a structure known to participate in olfactory memory (Heisenberg et al., 1985; Heisenberg, 2003). Stimuli consisted of common odorants at dilutions spanning several orders of magnitude (see Experimental Procedures).

Results

Oscillations and Phase Coding of Intensity

Hopfield (1995) has proposed an intensity-encoding scheme based on the phase of firing of principal cells relative to a global periodic signal. Because olfactory systems, including the locust AL (Laurent and Naraghi, 1994), display coherent oscillatory behavior in response to odors (Adrian, 1942; Freeman, 1978; Gray and Skinner, 1988) and because, in locusts, PN firing phase contains no information about odor identity (Laurent et al., 1996), we set out to evaluate the effect of odor concentration on AL oscillatory synchronization and on the firing phase of PNs. First, extracellular local field potential (LFP) recordings ($n = 38$, see Experimental Procedures) were made from the mushroom body, the target of the AL PNs (Figure 1A). Oscillatory potentials (20–30 Hz) were evoked when odorants were applied to the antenna, revealing coordinated, periodic PN activity, as previously described (Laurent et al., 1996; Wehr and Laurent, 1996). The oscillatory frequency remained constant [mean = 20.8 Hz, $f(3,198) = 0.67$, ns; data not shown], but oscillatory power increased significantly with concentration (Figure 1A), suggesting tighter PN

*Correspondence: laurentg@caltech.edu
[1]These authors contributed equally to this work.
[2]Present address: National Institutes of Health, NICHD, 49 Convent Drive, MSC 4495, Bethesda, Maryland 20982.

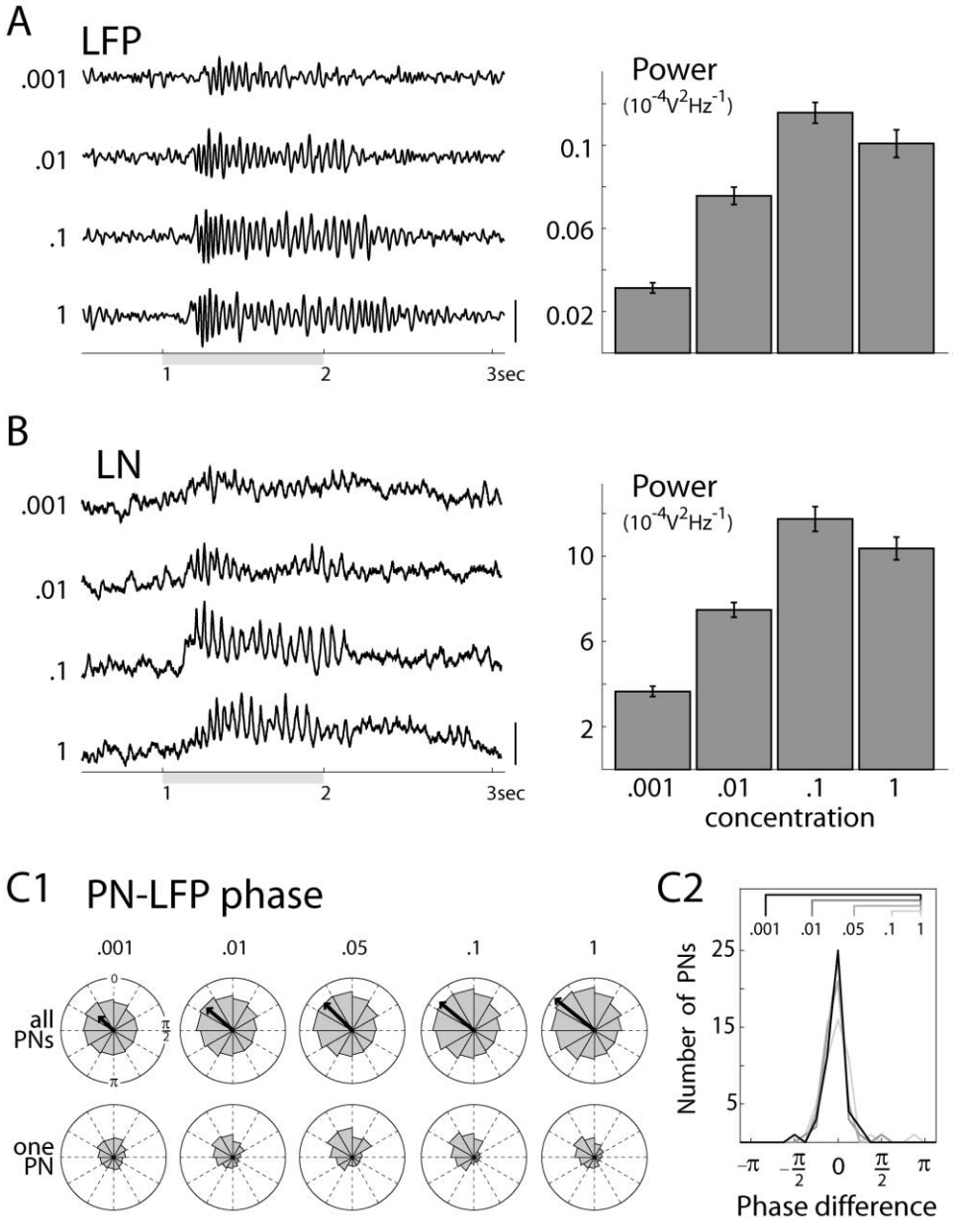

Figure 1. Network Oscillations and PN Phase Preference over Odor Concentrations

(A) Higher odor concentrations elicit greater oscillatory power in the local field potential (LFP) (see also Bäcker, 2002). LFP power measured over 1 s beginning with response onset. (Left) Examples of responses to hexanol from one experiment. Gray bar (here and throughout) indicates odor presentation. For display only, LFP was band-pass filtered, 5–55 Hz. Scale bar, 0.5 mV. (Right) Mean ± SEM response power from 38 experiments, ANOVA: $f(3,175) = 8$, $p < 0.0001$. LFP power slightly decreased at the highest concentration. The duration of the oscillatory response of the LFP also increased with odor concentration; ANOVA: $f(3,175) = 21.2$, $p < 0.0001$.

(B) LN oscillatory power also increased with concentration. (Left) Intracellular responses of an LN to cherry; low-pass filtered, 3 kHz. Scale bar, 8 mV. (Right) Mean ± SEM responses from 35 experiments, ANOVA: $f(3,162) = 9.5$, $p < 0.0001$.

(C1) PN spike phase preference (with respect to the LFP) is independent of odor concentration. (Top) All PNs: polar histograms (0 rad = peak of LFP cycle) show phase preference of 47 PNs responding to three odorants (octanol, hexanol, and geraniol); phase preference (arrow angle) was not significantly different across concentrations [cellwise ANOVA: $f(4,299) = 0.8$, ns] (see also Bäcker, 2002); vector strength (arrow length) increased with concentration. (Bottom) One PN: phase preferences of a single PN for responses to octanol; this PN spiked vigorously during the period of LFP oscillation for all concentrations. Phase preference did not change with concentration [spikewise ANOVA: $f(4,2773) = 2.1$, ns].

(C2) None of the 47 PNs examined showed a change in phase preference with odor concentration. For each PN, the preferred phase obtained with the highest concentration was subtracted from the phase obtained with the other four concentrations; all within-cell phase differences are plotted in the histogram. Within all PNs and across all concentration steps, an ANOVA detected no overall effect of concentration [$F(3,184) = 0.68$, $p = 0.56$]. Phase differences are all distributed normally around 0 (confirmed by individual unpaired t tests).

synchrony, increased global PN activity, or both (Laurent, 2002). Second, intracellular recordings were made from AL local neurons (LNs) (n = 35, Figure 1B, see Experimental Procedures), the inhibitory neurons responsible for PN oscillatory synchronization (MacLeod and Laurent, 1996). LN intracellular potentials also revealed an increase in oscillatory power with odor concentration (Figure 1B). This suggests that the increased LFP power at higher odor concentrations is due, at least in part, to stronger activation and periodic modulation of LNs. Third, extracellular (n = 47, see Experimental Procedures) recordings were made from PNs, simultaneously with LFP recordings. We found that the mean phase of PN spikes during odor responses was unchanged by stimulus concentration (Figure 1C); similar results were obtained with intracellular recordings. Thus, while global oscillatory power in the AL output increases with concentration, PN firing phase with respect to the ensemble response (LFP) appears not to be a coding variable in this system, at least within this range of concentrations.

PN Temporal Patterning and Concentration

Intracellular recordings from PNs (n = 39) showed that the slow temporal patterns evoked by odors (Laurent and Davidowitz, 1994) changed substantially and, sometimes, abruptly with concentration. Figure 2A shows the responses of one PN to four concentrations of cherry odor. At 0.001, this PN fired with a sustained train of action potentials followed by a long hyperpolarization. At 0.01, the excitatory segment of its response to that odor was slightly lengthened and the hyperpolarization reduced, indicating some continuity in response tuning across concentrations. At 0.1, however, the response changed substantially, now consisting of an early period of hyperpolarization followed by a train of action potentials. As the concentration was increased again, the PN's response profile changed little. This example indicates that the responses of PNs to odors are determined by competing excitatory and inhibitory inputs, whose timing and relative influence change, sometimes unpredictably, with stimulus concentration. We then carried out extracellular tetrode recordings from multiple PNs (n = 110 cells in 15 experiments, odorants adjusted to equalize vapor pressure, see Experimental Procedures). The changes in response patterns over odors and concentrations varied greatly across PNs; we could find no simple rule that, if applied to each PN, would allow us to predict the evolution of its responses across odor concentrations. Figure 2B shows the responses of 14 simultaneously recorded PNs to five concentrations of the three odorants, and Figure 2C shows the consistency of these responses over 15 trials with four PNs selected from the 14 in Figure 2B. Responses differed greatly across odorants (e.g., PN6, 0.001Ger, and 0.001Hex) but changed also with concentration (e.g., PN13). With some PN-odor combinations, spiking responses occurred earlier as the concentration was increased (e.g., PN13-Oct). For others, the converse was true (e.g., PN8 Hex). As observed with intracellular recordings, the changes from one response pattern to another could be abrupt as odor concentration was changed (e.g., PN8, 0.1- to 1.0Ger), but such discontinuities were not observed for the same concentration step in all PNs recorded simultaneously (e.g., PN13; 0.1- to 1Ger). This suggests that not all local AL interactions change for a given concentration step. Hence, odor identity and concentration appeared to be confounded in the response patterns of individual projection cells.

PN Mean Firing Rates and Concentration

We next examined mean PN response firing rates. In some PN-odor combinations, mean firing rates increased with concentration (e.g., PN13, Ger and Hex, Figure 2C). In others, firing rates were highest at the lowest concentrations (e.g., PN8-Oct, Figure 2C). The responses of 110 PNs (15 trials each) were pooled (Figure 2D), and mean response rates were measured over several intervals (1, 2, 3, or 4 s from stimulus onset) for all three odors and five concentrations; in all combinations, neither odor identity nor concentration had any effect on mean response rates (two-way ANOVAs, Figure 2E). This indicates that, while total afferent input to the AL increased with concentration (see Experimental Procedures; Joerges et al., 1997; de Bruyne et al., 2001), the summed output of the AL varied little over these concentrations. Hence, if stimulus concentration is represented downstream from the AL, we predict that it should require decoding the patterning of the AL output rather than its integrated intensity (see Figure 2E). In addition, this result suggests that the increase in LFP power with concentration (Figure 1A) results mainly from tighter synchronization of PNs (their preferred firing phase indeed sharpens with concentration; see vector strength, Figure 1C), itself related to (possibly as a cause and a consequence of) increased efficacy of inhibition (Figure 1B). The total AL output is thus adaptively regulated over input intensities.

Spatiotemporal Population Patterns

We sought to examine response patterns across the PN population, first, from groups of PNs recorded simultaneously (e.g., Figure 3A, left bracket, the same 14 PNs as shown in Figure 2B), and second, to better assess the ensemble response of the AL, from 110 PNs pooled from 15 experiments (Figure 3A, full set). In each experiment, the animal was given 15 trials each of five concentrations of the same three odorants, in random order (225 trials per experiment). Of these three odorants, two were structurally similar (hexanol and octanol) and both were dissimilar from the third (geraniol, a terpene). For each experiment, spikes were binned using two methods: (1) because PN output is decoded by Kenyon cells (KCs) over individual LFP oscillation cycles (Perez-Orive et al., 2002), we binned the spikes by LFP oscillation cycle (50 ms per cycle on average, see Experimental Procedures); (2) we measured spike counts in consecutive 50 ms bins independent of LFP cycle boundaries. Each trial was represented as a high-dimensional vector of spike counts; each vector had $k = n \times m$ dimensions, where n is the number of PNs considered (up to 110), and m is the number of time bins (e.g., $m = 20$ for 50 ms bins over a 1 s response period). Each vector thus represented the spatiotemporal pattern defined by the responses of n PNs over time in a single trial. We then analyzed the similarities between the vectors representing all trials; because first trial responses differ greatly

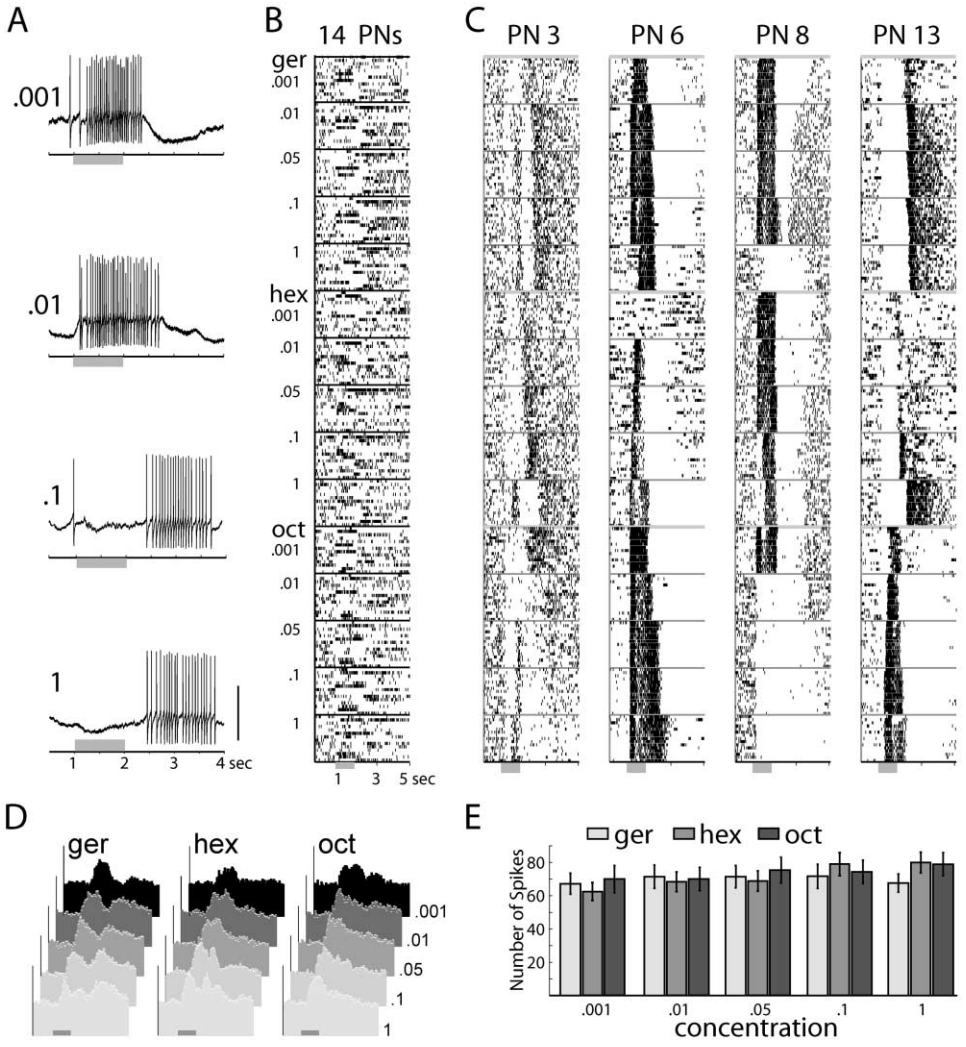

Figure 2. PN Responses to Different Odorants and Concentrations

(A) Examples of responses to cherry from one experiment. Intracellular recordings of a single PN reveal concentration-specific interplay of excitation and inhibition, leading to temporal patterns that are consistent from trial to trial (see [C]). Odor pulse, 1 s; scale bar, 35 mV.

(B) Ensemble view: spike time raster of simultaneous "tetrode" recordings from 14 PNs firing in response to five concentrations each of three odorants: geraniol (ger), hexanol (hex), and octanol (oct). Only the tenth trial (of 15 for each odor-concentration pair) is shown; within the horizontal separator lines, each row is a different PN. Odorants delivered in a randomized sequence.

(C) Selected PNs from (B). Within separator lines, each row is a different trial (from top to bottom).

(D) Summed PN response profiles change moderately with odorant and concentration. 110 PNs (15 experiments), 15 trials per condition, 100 ms bins.

(E) Mean response intensity is constant across odors and concentrations. Pooled responses of 110 PNs; mean response rates measured over 1, 2, 3, or 4 s from stimulus onset (1 s shown) for all three odors and five concentrations; in all combinations, odor identity or concentration had no effect on mean response rates [two-way ANOVA for data shown: $f_{concentration}(4,1635) = 0.92$, ns; $f_{odor}(2,1635) = 0.40$, ns; $f_{interaction}(8,1635) = 0.39$, ns].

from the others (Laurent and Naraghi, 1994; Stopfer and Laurent, 1999), they were excluded, giving us 14 trials $\times$ 5 concentrations $\times$ 3 odors $=$ 210 vectors. We will first examine the results obtained with groups of PNs recorded in single experiments and later consider results from the composite set of 110 PNs.

We applied principal component analysis (PCA) (see Experimental Procedures [Turk and Pentland, 1991; Joliffe, 1986]), a linear dimensionality reduction method, on the sets of simultaneously recorded PNs. The reduced data revealed odor- and concentration-specific structures in the spatiotemporal patterns that were not seen in individual PN responses. Visualizing the results using, for illustration purposes, the first three principal components (see Experimental Procedures), we found that the response patterns elicited by each odor formed distinct clusters (Figure 3B1). An unsupervised hierarchical clustering algorithm applied to the first eight principal components (see Supplemental Figure S1 available online at http://www.neuron.org/cgi/content/full/39/6/991/DC1) of these data (see Experimental Procedures) confirmed the existence of this structure and revealed further substructure in the response patterns (Figure 3B2). Responses clustered by concentration (with some

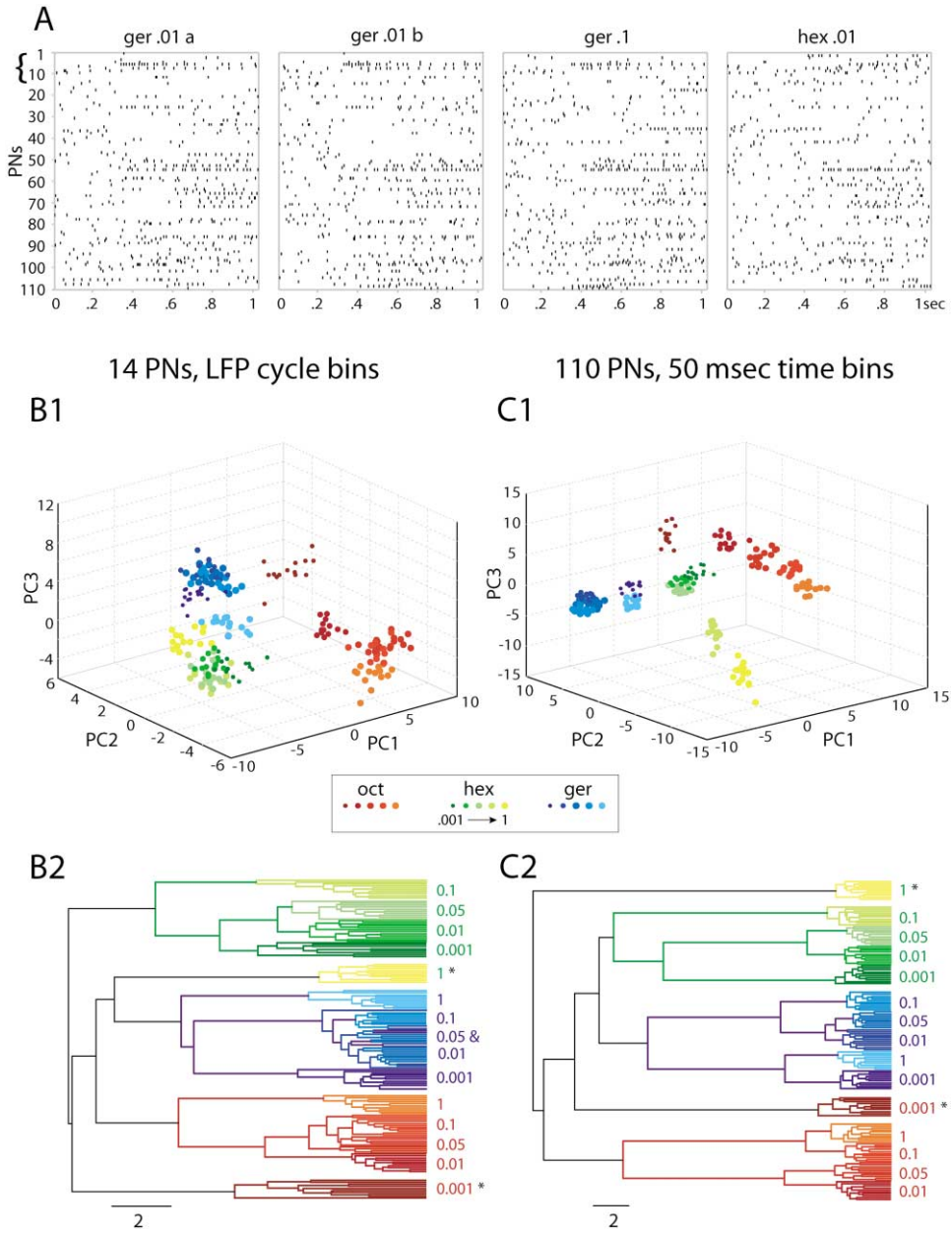

Figure 3. PN Ensemble Spatiotemporal Patterns Cluster by Odorant and Concentration

(A) Representative ensemble responses (shown as raster plots, each row is a different PN) to two odorants, presented at two concentrations, throughout the time shown. The first 14 PNs (bracket at left) were recorded simultaneously in one experiment (see [B]). The rest were obtained in 14 other experiments. Repeated presentations of ger .01 (a and b) elicited very similar ensemble responses; a different concentration (ger .1) elicited a somewhat different response; a different odorant (hex .01) elicited a very different response.

(B1) Spatiotemporal responses from 14 simultaneously recorded PNs (bracket at left in [A]) to five concentrations of three odors projected onto the space of the first three principal components (PC1-3). Spike counts were measured in bins defined by the simultaneously recorded LFP oscillation cycle. Each dot represents an ensemble response such as shown in [A]. The distribution of variance is discussed in Experimental Procedures.

(B2) Hierarchical clustering of the reduced data (eight PCs) shows that individual trials cluster by concentration; concentration groups then cluster by odor. Asterisks (*) identify the two exceptions.

(C1) Same analysis as in (B1) but using all 110 PNs (pooled from 15 animals). Spike counts for individual PNs were measured in 50 ms bins.

(C2) Same as in (B2), with set of 110 PNs from (C1).

mixing among close concentrations), and concentration groups then clustered by odor, with a couple of exceptions (asterisks) for one very high and one very low concentration (Figure 3B2). We assessed the clustering using simple classification algorithms (tests A and B, see Experimental Procedures) based on the first eight principal components and Euclidian distances. For the experiment shown, we could classify individual re-

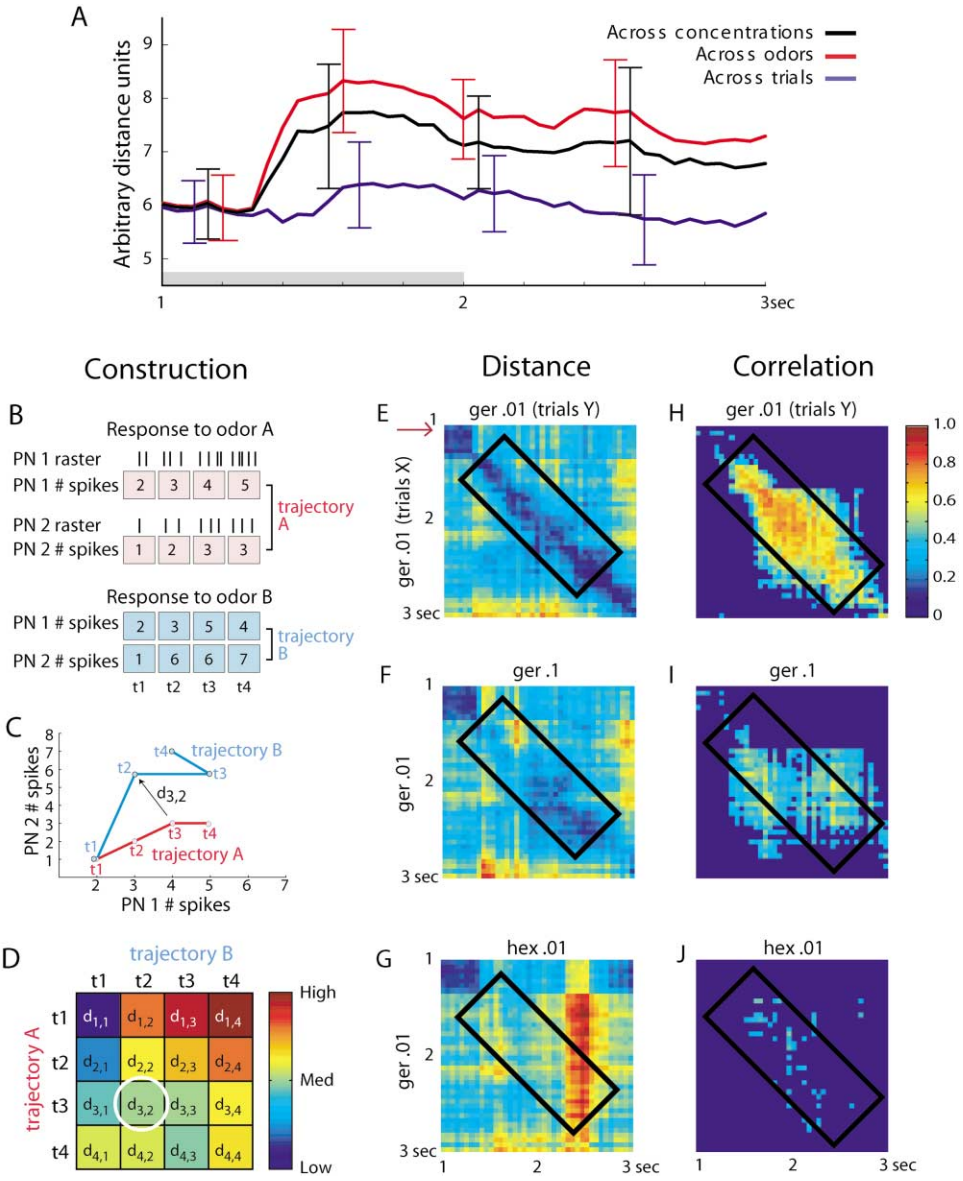

Figure 4. Quantifying Differences among Response Patterns as They Evolve over Time

(A) Average Euclidean distances (±SD) calculated for each 50 ms time slice, across 110 PN vectors. Across trials, same odor-concentration pair; across concentrations, same odor; across odors, same concentration.

(B–D) Procedure to construct trajectories from individual spike trains (artificial data).

(B) Spike counts for individual PNs are measured in bins of given width over the time of the response. When stacked together across PNs, this produces a series of time slice vectors, each of a dimension equal to the number of PNs included. These vectors, when linked in sequence, produce trajectories that represent the evolution of the PNs' states in the high-dimensional space of PN spike counts.

(C) The two trajectories corresponding to example in (B). Euclidean distance between different trajectories can then be measured between any two high-dimensional time slices (in this two-dimensional example, $d_{3,2}$ is the distance of the time slice of trajectory A at time t3 to the time slice of trajectory B at time t2).

(D) Matrix of Euclidean distances, calculated as in (C). Each pixel $d_{i,j}$ represents the color-coded distance between the time slice i of trajectory A and time slice j of trajectory B. Diagonal represents the distance between time-matched time slices of trajectories, and each row represents the distance from a particular time slice of trajectory A to all others of trajectory B.

(E–G) Real data, distance matrices calculated from 110 PN data set in Figure 3C; bin width, 50 ms, averaged over three trials. Of all possible matrix permutations, only three examples are given.

(E) Distance matrix calculated as in (C), between 110-D vectors taken from different sets of trials of 0.01 geraniol stimulation. Stimulation onset, 1 s; PN response onset is ~300 ms later, owing mainly to delays in odor propagation and olfactory transduction. The first row (arrow) shows distances from a time slice in the baseline period to the subsequent time slices. Distance is initially minimal (dark blue) until ~300 ms after stimulus onset, when the system begins to respond. Blue pixels around diagonal (black box) show that distances between nearby time slices across trials are low even when the ensemble response has moved away from baseline, indicating that PN ensemble response changes gradually from one time slice to the next.

(F) Distances between responses to two concentrations of the same odorant, 0.01 geraniol and 0.1 geraniol. Increase in distance from baseline state after 400 ms is greater than in (E) (first row, yellow and orange pixels). However, time-matched time slices are still somewhat

sponses as belonging to the correct concentration group with >90% success (test A, see Experimental Procedures) and individual concentration subclusters as belonging to the correct odor group with >90% success, even after all trials with the tested concentration had been excluded from the template set (test B, see Experimental Procedures). These results were qualitatively similar across all experiments with comparable numbers of PNs, but we found tighter clustering and greater classification success for experiments with larger numbers of simultaneously recorded PNs. For sets of simultaneously recorded PNs, the results, while qualitatively similar for both binning methods, were quantitatively better (by up to 10%) when spikes were binned with respect to the simultaneously recorded LFP cycles (data not shown).

The locust has over 800 PNs per antennal lobe, from which we can presently record, at best, 25 simultaneously. In an effort to better approximate the response of the entire antennal lobe, we next analyzed odor response profiles from 110 PNs pooled from 15 tetrode experiments (e.g., composite raster in Figure 3A; see Discussion). Spike counts were measured in consecutive 50 ms bins to produce population vectors (110 PNs $\times$ 20 bins $=$ 2200 dimensions for 1 s patterns).

When we applied PCA to this data set, the reduced data once again revealed odor- and concentration-specific structures in the spatiotemporal patterns. Using three PCs for visualization, we found not only that the response patterns elicited by each odor formed distinct clusters (Figure 3C1) but that each odor cluster contained within it smaller subclusters of response patterns evoked by the different concentrations. Hierarchical clustering using eight PCs (see Experimental Procedures) showed that responses now clustered nearly perfectly by concentration (Figure 3C2), and concentration groups clustered by odor, with the same two exceptions (asterisks). We could classify individual responses as belonging to the correct concentration group with 100% success (test A) and individual concentration subclusters as belonging to the correct odor group with >90% success (test B). In conclusion, odors appear to evoke distributed spatiotemporal patterns in which many neurons contribute to encoding both concentration and identity; the firing of the PN population analyzed over individual PNs and over time (with oscillation-cycle length resolution) can be used by an observer to identify both concentration and identity.

Analysis and Visualization of the Spatiotemporal Patterns

Recent results indicate that, during an odor presentation, PN output is decoded by KCs over individual LFP oscillation cycles at a rate of 20–30 Hz (Perez-Orive et al., 2002). In a given KC, these periodic epochs of integration each seem to be independent of the preceding ones, owing to a periodic inhibitory reset of KCs after each oscillation cycle (Perez-Orive et al., 2002). From this we infer that quantifying the response of a PN over the entire duration of a stimulus (e.g., by integrating its total discharge or by quantifying its patterned response over a long time, as in Figure 3) is probably not a functionally relevant approach. The PNs' output should rather be interpreted from the perspective of their targets, i.e., piecewise. The following analysis attempts to identify, from PN population patterns analyzed over oscillation-cycle lengths, the features that might differentially encode odor concentration and identity.

We examined the PN population output as time series of 110-D vectors (110 PN data set in Figure 3), sampled in consecutive 50 ms "time slices." To track the evolution of the different odor responses, we calculated average Euclidean distances (in 110-D space) between time-matched vectors, i.e., one slice at a time (Figure 4A). The PN assembly responded fairly consistently over repeated trials with the same odor and concentration (blue, Figure 4A). When the concentration alone was changed, however, the patterns diverged, evident as increased average distances between corresponding time slices (black, Figure 4A). When the odor itself was changed, the ensemble responses diverged even further (red, Figure 4A). Because the patterns of PN activation changed over time, we also examined, for each response, differences between slice vectors measured at different times. A matrix of Euclidian distances (calculated as in Figures 4B–4D) showed that distances between vectors were small (dark blue) during the baseline period but were larger between baseline and slices 400–500 ms after stimulus onset (light green and yellow) (Figures 4E–4G). Note, however, that the distances between neighboring time slices after the response had started (flanking the diagonal, box, Figure 4E) were small when comparing trials in the same odor concentration series. This indicates that the sets of firing PNs are updated incrementally over the duration of each response. In addition, distances between time-matched and neighboring slices across nearby concentrations of the same odor (Figure 4F) were smaller than those across different odors at the same concentration (Figure 4G). This suggests a greater overlap between the sets of firing PNs during the response to different concentrations of an odor than between PN sets activated by different odors. We also carried out a similar analysis using correlations rather than distances (Figures 4H–4J). Matrices showing significant ($p < 0.001$) correlations between time slice vectors also showed the same trends (Figures 4H–4J). Our goal thus became to visualize, in just a few dimensions, an approximation of the trajectories defined by the evolving responses of the 110 PNs to each odor and concentration.

Locally linear embedding (LLE) (Roweis and Saul,

similar to each other across responses to different-concentration stimuli (blue and green pixels around diagonal, box).
(G) Distances between the responses to different odorants, 0.01 geraniol and 0.01 hexanol. Distance at baseline is minimal; the increase in distance after the system begins to respond (first row) is comparable to those in (E) and (F), indicating that they are all at roughly comparable distances to baseline during the period of the response. A significant difference is observed around the diagonal: yellow and red pixels (box) indicate that the responses to the two different odors at the same concentration are very different from each other.
(H–J) Normalized correlation matrices matching the Euclidean distance matrices (E–G). All correlations shown are significant ($p < 0.001$).

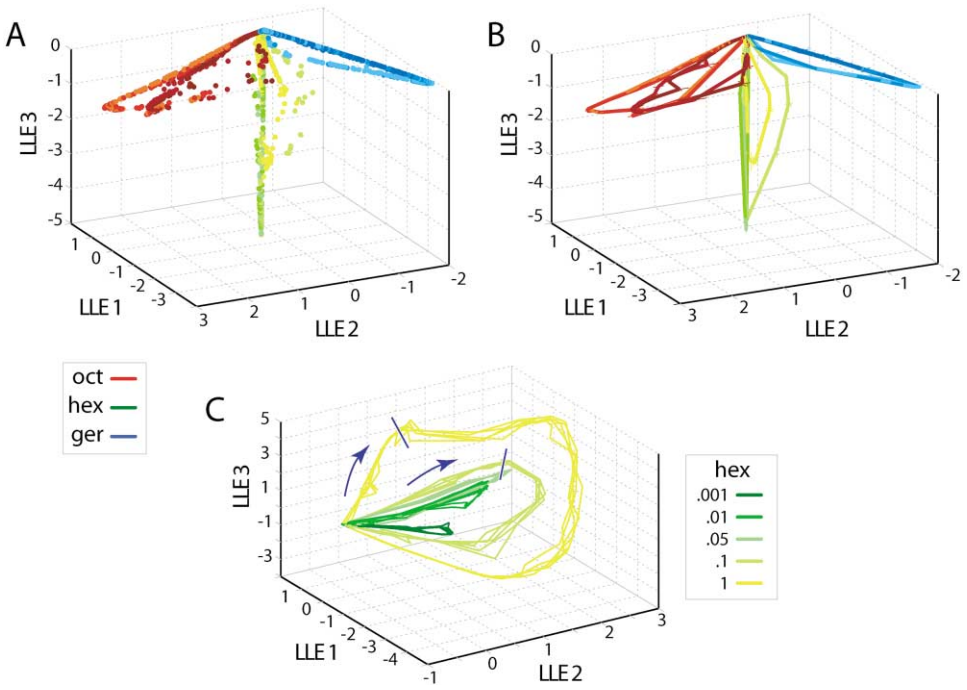

Figure 5. Visualization of Trajectories Representing PN Population Response over Time

(A) Time slice points calculated from 110 PN responses to four concentrations (0.01, 0.05, 0.1, 1) of three odors, projected onto three dimensions using locally linear embedding. Shown are 60 time slice points per trajectory (6 s total, beginning 1 s before stimulus onset, 100 ms bins, averaged over three trials).

(B) Time slice points in (A) were connected in sequence to visualize trajectories. Initially in a resting state (origin of the coordinate system), the system responds with stimulus-specific trajectories. The trajectories in response to different concentrations of the same odor remain on the same (odor-specific) manifold. Five-trial averages for each odor-concentration pair; lines at vertices indicate SD.

(C) Trajectories corresponding to responses to five concentrations of hexanol, projected onto three dimensions using LLE. Arrows, direction of motion; blue lines, time of stimulus offset, shown for two concentrations. Five trajectories (each an average of three trials, 15 trials per odor-concentration pair) for each concentration are shown. These overlapping trajectories are separate from those of other concentrations.

2000), an unsupervised nonlinear dimensionality reduction technique well suited to uncovering low-dimensional structure present in high-dimensional data (see Experimental Procedures; Seung and Lee, 2000), was used to visualize (here in three dimensions, Figure 5A) the successive time points representing the states of the 110 PNs in response to multiple concentrations of the three odors. When connected in temporal order (Figure 5B), these points formed closed and stimulus-specific trajectories away from the initial resting state upon stimulus onset and back to rest some time after the stimulus ended. In agreement with the Euclidean distance measurements, the trajectories representing responses to different concentrations of an odor remained close to one another (forming odor-specific manifolds) but far from those of other odors. The trajectories and manifolds appeared connected only at rest. We also applied LLE to a data set obtained with just one odor (e.g., hexanol, Figure 5C). This embedding suggested that odor-evoked patterns move progressively further away from the resting state (baseline) as the concentration is increased. Trajectories representing higher concentrations appeared to take longer to return to the rest state. The antennal lobe network can thus be described as a dynamical system that responds to stimuli by moving away from its baseline state, in what can be visualized as concentration-specific trajectories on odor-specific manifolds. These manifolds exist because of concentration-invariant features (similarities in the sets of transiently coactivated PNs) in the odor-evoked PN ensemble activity patterns. These features, which appear only with multi-PN data and can be most clearly seen in this compressed representation (Figures 5B and 5C), resolve the apparent confounding of identity and concentration in single PN data (Figures 2A–2C).

Decoding Cycle by Cycle

Given that KCs assess the state of PNs cycle by cycle during a response (Perez-Orive et al., 2002), we wanted to estimate the information content of the PN assembly for individual cycles at successive times along the trajectories. We used PCA to reduce the dimensionality of individual 50 ms slices, one slice at a time. We found that, at certain times during odor presentation, responses once again clustered by odor identity (e.g., see Figure 6A, showing the first three PCs). Hierarchical clustering using eight principal components (Figure 6B) showed that responses clustered in concentration groups, with some exceptions (primarily mixing among responses to nearby concentrations of the same odor) and that concentration groups clustered by odor (again, with some exceptions, see asterisks). Individual time slice reconstructions of odor responses using eight principal components (Figure 6C, see also Supplemental

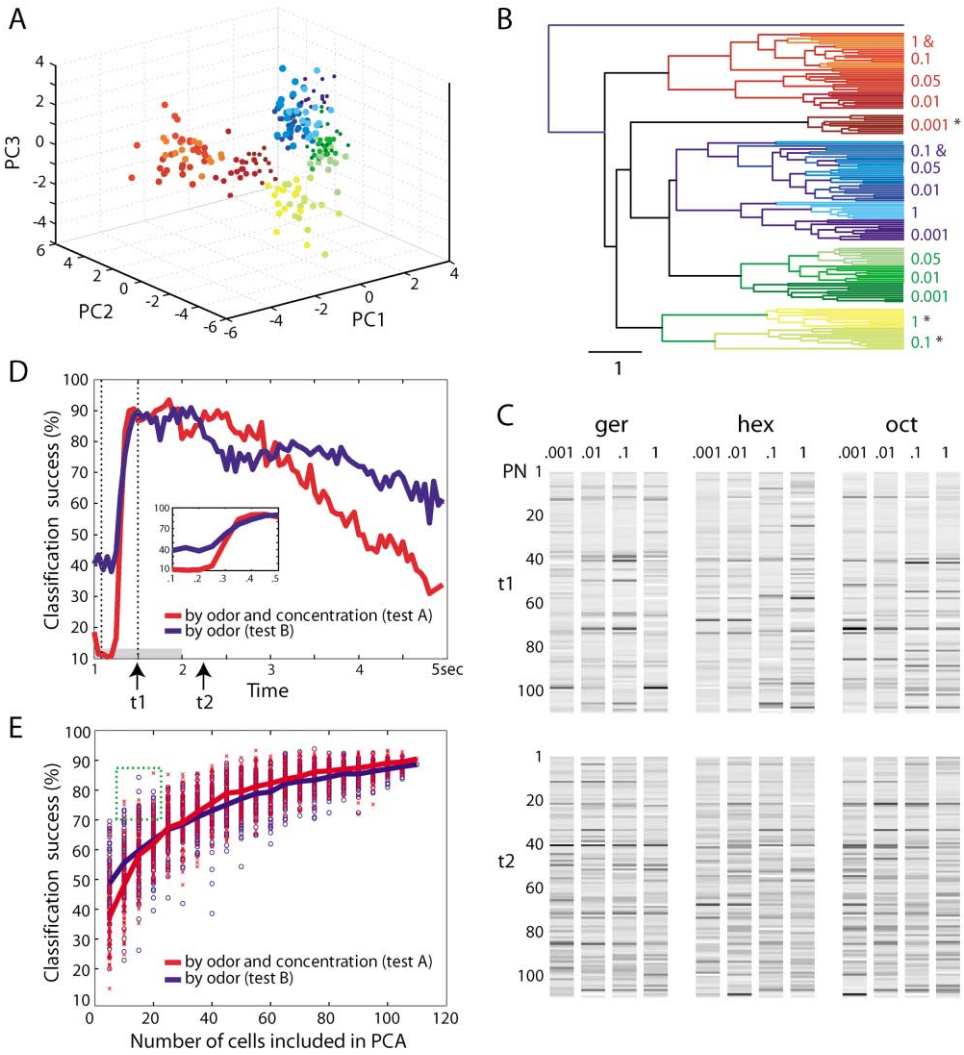

Figure 6. Classification by Single Cycle-Length Time Slices

(A) Points from the 50 ms time slice 0.5 s after stimulus onset; 110 PN set projected onto space of first three principal components. Points cluster by odor and concentration.

(B) Hierarchical clustering shows that points from the time slice in (A) largely cluster by concentration; concentration groups then cluster by odor, with some exceptions (indicated by *).

(C) Reconstructions of PN activity states in two time slices (t1 = 0.5 s; t2 = 1.25 s after stimulus onsets; see [D]) using eight PCs show significant positive contributors (darker pixels indicate higher spike counts) for different odors and concentrations. The set of PNs active in response to a particular odor-concentration pair (column) changes over time (t1 and t2 rows), although vectors from either time slice can be classified successfully by both odor and concentration (arrows in [D]).

(D) Classification success with single (50 ms) time slices stays high well into the response. (Inset) Evolution toward peak classification performance is attained within 200–300 ms after the response begins.

(E) Classification success as a function of the number of PNs included in the time slice. Small numbers of PNs sufficed for good classification only for a few PN combinations (top points in each distribution, outlined in green box for the 10 to 20 PN range).

Figure S2 at http://www.neuron.org/cgi/content/full/39/6/991/DC1) revealed subsets of PNs that preferentially contributed to particular features of the representation (identity, concentration); these subsets, however, changed over time (e.g., $t_1 = 1.5$ s and $t_2 = 2.25$ s, Figure 6C). Classification of responses into odor groups was 90% successful for many time slices all through the response (Figure 6D), with errors in some of the lowest and highest concentration groups. Classification into concentration subclusters was only slightly less successful on average (tests A and B, see Experimental Procedures). The evolution toward peak classification success occurred very rapidly (200–300 ms) (inset, Figure 6D), and there appeared to be sufficient information for both identity and concentration to be decoded by an observer over single cycles well into the response. Classification success using only subsets of the 110 PNs (100 random samples of 5, 10…100 PNs each) is shown in Figure 6E (see Experimental Procedures). Whereas the distribution of success rates was broad for all PN subset sizes, a few random PN combinations (top points of each distribution, e.g., green box, Figure

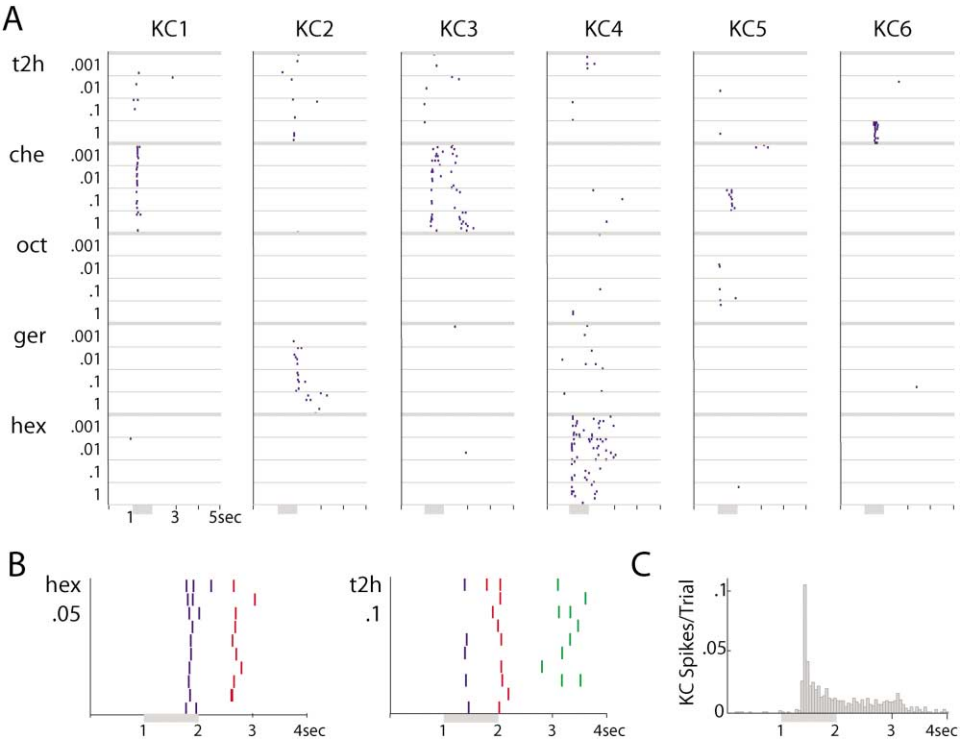

Figure 7. KCs Respond to Specific Odors or Specific Concentrations of Odors

(A) Rasters show examples of KC response specificity. KCs 1-4 responded reliably to a range of concentrations of an odor; KCs 5-6 responded to only one tested concentration of one odor. KCs 1, 3, 4, and 5 were recorded simultaneously in one preparation; KCs 2 and 6 were recorded simultaneously in a different preparation. t2h, trans-2-hexanal; che, cherry.

(B) KCs fired at different, favored times after odor onset. (Left) Superimposed rasters of two simultaneously recorded KCs (red, blue rasters), both responding to .05 hexanol. (Right) From a different experiment, three simultaneously recorded KCs (blue, red, green rasters), all responding to .1 trans-2-hexanal.

(C) Histogram of response times for all KCs with stimulus-specific responses.

6E) reached success rates between 75% and 90% for subsets containing as few as ten PNs. Hence, enough information about stimulus identity and concentration (in the range tested) can be found by an observer in small PN subsets, provided that the right PNs are considered.

Concentration Tuning and Invariance of KCs

We estimate that 50,000 KCs each receive inputs from 10 to 20, on average, of the 830 AL PNs (Perez-Orive et al., 2002), but the structure of this connectivity matrix is so far unknown. If each KC is connected to a subset of PNs that, for the appropriate stimulus, is coactivated within the same cycle or cycles, that KC's responses should reflect the variations (across odors and concentrations) of coactivity of the PNs connected to it. That is, some KCs might respond to a narrow concentration range of one odor while others would be relatively indifferent to concentration (invariant), reflecting the combined sensitivities of their presynaptic PNs. Further, if KCs decode PN output over LFP cycle-length epochs, we would predict that KC responses should occur at cell- and stimulus-specific times during each response.

We recorded from many KCs simultaneously (total of 133 KCs in 17 experiments) while stimulating the animal with different odors and concentrations. KC responses were brief and rare (Perez-Orive et al., 2002) but, when found, displayed the predicted kinds of specificity (Figure 7A). Some KCs (~30%, e.g., KC6) responded selectively to specific concentrations of particular odors, others (~15%, e.g., KC1) to one odor across a contiguous range of concentrations, and a few in less-specific ways still. Also, the timing of KC responses relative to the stimulus onset differed across KCs and stimuli (Figure 7B), consistent with the finding that decoding of the PNs' output occurs both piecewise (Perez-Orive et al., 2002) and throughout the stimulus duration (Figure 7C). These results indicate that odors are represented in the mushroom body by identity-selective sets of KCs, containing cells with different degrees of concentration invariance. The observed degrees of selectivity (to odor identity and concentration) are consistent with the amount of information present in a small proportion of randomly chosen assemblies of 10 to 20 PNs (Figure 6E).

Discussion

Pooling: Technical Considerations

PNs recorded in several animals were pooled for some of our analyses (Figures 3C, 4, 5, and 6). Is this pooling strategy well founded? We will assume that the set of pooled PNs approximates a large sample from a single locust if the following conditions are met. (1) Different locusts should have similarly tuned PNs. While this condition has not been resolved for locust, morphological studies in *Drosophila* suggest that PNs in that insect

are indeed identifiable across animals (Wong et al., 2002; Marin et al., 2002). This interindividual morphological identifiability in *Drosophila* is paralleled by physiological properties and odor tuning (R.I. Wilson and G.L., unpublished data). Many neurons in locusts are also identifiable from animal to animal (Burrows, 1996). In the absence of evidence to the contrary, we assume that PN populations are very similar across individual locusts. (2) The pooled set should not contain many "duplicate" PNs (i.e., the same PN from different animals represented more than once). Two lines of evidence suggest that our set contains very few duplicates. First, a probabilistic analysis based upon the number of PNs in one locust ($\sim$830), the number of PNs sampled per experiment (2 to 14), and condition (1) above shows that the probability of repeatedly sampling many PNs across experiments is very small (see probability distribution in Supplementary Figure S3 at http://www.neuron.org/cgi/content/full/39/6/991/DC1). Second, the 110 PNs in the pooled set had distinct response tunings when assessed on the three odors tested (see Figure 6C). While we cannot be certain that the pooled set is identical to a large sampling of PNs in a single individual, all available data suggest that conditions (1) and (2) above are met.

Gain Control and Absence of Phase Encoding

Imaging data indicate that the total afferent input to the AL (and OB) increases with odor concentration (Ng et al., 2002; Wang et al., 2003; Cinelli et al., 1995; Friedrich and Korsching, 1997; Joerges et al., 1997; Meister and Bonhoeffer, 2001; Rubin and Katz, 1999; Stewart et al., 1979); yet, the total AL output, integrated across PNs and time, does not change significantly over a 1000-fold increase in odor concentration. This indicates the existence of adaptive gain control within the AL, consistent with the observed increased modulation of LNs over concentrations. This apparent involvement of LNs in controlling PN output is also consistent with the increased synchronization of PNs with odor concentration. Whereas oscillatory synchronization is relevant for behavioral discrimination (Stopfer et al., 1997) and for decoding by KCs (Perez-Orive et al., 2002) and their downstream neurons (MacLeod et al., 1998), there is so far no experimental evidence for a phase code (with respect to the LFP) for concentration (see Hopfield, 1995). Other investigators suggest that response latencies with respect to the slower respiration cycles (rodent olfactory bulb; Spors and Grinvald, 2002; Margrie and Schaefer, 2003; Cang and Isaacson, 2003) could be used as features in odor concentration coding; in insects, odor sampling is not coupled to respiration. In conclusion, as in other systems, AL circuits adapt their mean output to dramatically compress input levels (Wachowiak et al., 2002); unlike other systems, however, AL circuits reflect—and transmit information about—input intensity through variations in the spatiotemporal patterning of their output, which are decoded by downstream neurons (see below).

Concentration Clusters within Identity Superclusters

As observed in other animals (Kauer and Moulton, 1974; Meredith, 1986; Wellis et al., 1989), the patterned responses of single AL principal neurons depend both on odor identity and concentration. Thus, steps in concentration of one odor can evoke single-PN response pattern changes indistinguishable from changes caused by a change in odor identity. Information about both odor identity and concentration, however, can easily be separated when odor representations are considered as evolving instantaneous vectors of activity across many PNs (i.e., sets of transiently coactive PNs), an analysis consistent with the known properties of their targets, the KCs (Perez-Orive et al., 2002). The activation patterns across the PN population are such that the abstract "coding space" can be thought of as divided into regions representing odor identities, each consisting of ordered subregions representing odor concentrations. The representation of an odor at very low or very high concentrations occasionally differed significantly from the others within its cluster. We predict that perceptual discontinuities should occur at these transitions; this needs to be tested behaviorally.

Differences between Concentration and Identity Patterning

These data extend our proposed spatiotemporal models for odor representations (Laurent, 2002; Laurent et al., 2001; Rabinovich et al., 2001) and for temporal decorrelation (Friedrich and Laurent, 2001; Laurent, 2002). Odor representations can be described as sequences of odor- and concentration-specific PN activity patterns, or trajectories. Trajectories representing different concentrations—within the range examined—of the same odor lie next to one another, implying that they share common elements (that is, PNs and times of coactivation). These families of trajectories define low-dimensional structures (manifolds) (Figures 5B and 5C). How can this population view be reconciled with the results of single-PN recordings (Figures 2A–2C) that indicate discontinuities?

When the concentration of an odor was changed, individual PN response patterns to an odor could change suddenly and drastically with certain concentration steps (Figure 2). These changes, however, did not occur at the same concentration steps across all PNs. Hence, trajectories (i.e., the high-dimensional state of the PN assembly over time) corresponding to different concentrations of an odor remained close to one another (because most changes in PN responses were relatively small when seen over the population). Each family of such nearby trajectories thus defines an odor manifold. Manifolds represent the degree of concentration invariance across the PN population responses for particular odors; they reflect the relative continuity in PN population responses across concentrations of an odorant, something that is not apparent in the responses of individual PNs, which often show discontinuities (see Figure 2C).

By contrast, when the identity of an odor was changed, a greater proportion of PNs changed their responses significantly, explaining the larger distances between resulting odor trajectories, and thus defining distinct manifolds. The key difference, therefore, between individual PN response patterns evoked by odor identity and by concentration appears to be not the extent of the pattern change per PN but rather the probability that such significant changes will co-occur across

many PNs for a given change in the stimulus. For a 10- to 1000-fold change in concentration, this probability is low. For a change in identity, it is generally high.

PN Patterning Is Consistent with KC Selectivity

The selectivity of the postsynaptic KCs to odor intensity could be explained by their connectivity to particular sets of PNs. A KC connected to PNs that are largely coactive (during a given oscillation cycle) across many concentrations should be concentration invariant within that range. By contrast, a KC connected to PNs that are not coactive across concentrations should be more selective. We found KCs of all concentration specificities, suggesting a diversity of PN-KC connection patterns. Given 830 PNs, 50,000 KCs, and an estimated fan out of 1PN:600KCs in locust (Perez-Orive et al., 2002), there exists an enormous number of possible connectivity matrices between the two populations. This connectivity has yet to be characterized.

Each KC integrates PN output cycle by cycle (50 ms mean cycle duration) and over 10 to 20 PNs on average (Perez-Orive et al., 2002). Many individual 50 ms time slices across the 110 PNs were sufficient to discriminate between odors and concentrations in our sample. If the number of PNs was reduced, however, discrimination became possible only with some PN subsets (Figure 6E), consistent with the observed rarity of KC responses (Perez-Orive et al., 2002).

Maximum distances between representations were, on average, reached within 200–300 ms of PN response onset. At response onset, LFP oscillation frequency is generally around 30 Hz (Laurent and Davidowitz, 1994; Laurent and Naraghi, 1994), indicating that maximum divergence between representations can be reached within five to ten oscillation cycles or steps of AL processing, a process apparently faster than that described for zebrafish (Friedrich and Laurent, 2001). The processes internal to the AL that generate this divergence must therefore be tuned to be both dynamically unstable—to allow this fast divergence (e.g., Rabinovich et al., 2001)—and yet well controlled—to enable the representations of different concentrations of one odor to diverge less than those of different odors. How this remarkable equilibrium is achieved remains to be understood.

Experimental Procedures

Odorants

For experiments with intracellular recording, odorants [monomolecular, including 1-hexanol, 1-heptanol, cis-3-hexen-1-ol, trans-2-hexen-1-ol, hexanal, 2-heptanone, 1-octanol, and geraniol (Sigma) and 3-pentanone, (Aldrich); and blends: mint and cherry, (LorAnn Oils), neat, or serially diluted in mineral oil (J.T. Baker) to yield stimuli at 0.001, 0.01, 0.1, or 1× of full strength] were applied to small strips of filter paper and placed in cartridges in series with separate pipettes (1 cm diameter). Puffs of desiccated and filtered air (1 s, 20s-1) carried the contents of the cartridges' headspace past the antenna (distance, 1 cm). A large vacuum funnel behind the antenna maintained a steady flow of background air and quickly removed the odorants. For experiments with tetrodes, octanol, hexanol, and geraniol were mineral oil dilution-standardized by vapor pressure in accordance with Raoult's law and then serially diluted in mineral oil to yield strengths 0.001, 0.01, 0.05, 0.1, or 1× that of the standard. To the experimenter, the highest concentration smelled sharp and distinct; the lowest was too weak to be detected. KCs were typically tested with a larger set of odors, to increase chances of detectable responses. Twenty milliliters of each odorant was placed into a glass vial (60 ml). The headspace content was carried by puffs of desiccated and filtered air (0.3 l/min, 1 s, 20s-1) into a teflon tube (1 cm diameter) to mix with a constant stream of air (0.3 l/min) directed to the antenna (distance, 1 cm). A large vacuum funnel behind the antenna removed odorants.

Electrophysiology

Results were obtained from 54 male and female locusts (*Schistocerca americana*) raised in a crowded colony. Young adults were immobilized with one antenna intact and fixed in place. The brain was exposed, desheathed, and bathed in locust saline, as previously described (Laurent and Naraghi, 1994; Stopfer and Laurent, 1999). LFPs were recorded either using saline-filled blunt glass micropipettes (tip, ~10 μm, ~10 MΩ), amplified with a d.c. amplifier (NPI, Adams-List), or using custom wire tetrodes, amplified with a custom d.c. amplifier.

Intracellular recordings from antennal lobe neurons were made using 0.5 M potassium acetate-filled sharp glass micropipettes (~150 MΩ, Sutter P87 horizontal puller) and amplified with a separate d.c. amplifier (Axon Instruments). Intracellular data were acquired using NBM116L hardware and LabVIEW (National Instruments).

Tetrode data with PNs were acquired using silicon probes from the Center for Neural Communication Technology (Drake et al., 1988); KC data were acquired using custom twisted wire tetrodes (Perez-Orive et al., 2002). PN and KC spikes were sorted offline using an algorithm (Pouzat et al., 2002) implemented in Igor (WaveMetrics Inc.). Because LNs do not produce sodium action potentials (Laurent and Davidowitz, 1994), all spikes in the AL were unambiguously attributed to PNs. KC somata are found in a layer containing no other cell type. All spikes recorded in this layer of 50,000 somata were thus unambiguously assigned to KCs. Only the records from unambiguously separated clusters (see quantitative criteria in Pouzat et al., 2002) were kept and analyzed (PNs and KCs). Samples can be seen in Supplemental Figure S4 at http://www.neuron.org/cgi/content/full/39/6/991/DC1. Results were analyzed with MATLAB (The MathWorks Inc.) software.

Data Analysis

Statistical comparisons were made by unpaired t tests and one- and two-way analysis of variance with significance level set at $p < 0.05$. LFP and LN power was estimated by integrating a 15 Hz band centered on each preparation's peak odor response frequency. Power spectra were calculated from unfiltered records.

Principal component analysis (PCA) was performed using functions from MATLAB's Statistics Toolbox (The MathWorks Inc.). Observation of the "elbow" of the scree plot and the "broken stick rule" (Joliffe, 1986) led us to retain the first eight principal components (PCs) for further analysis; we used the first three PCs for display purposes. In general, for the k dimensional vectors representing single trials ($k = n$ PNs $\times m$ bins; $m = 20$ for Figure 3, $m = 1$ for Figure 6), the variance captured by the first few PCs was low (24% and 30% for three and eight PCs, respectively, in Figure 3B; 8% and 33%, respectively, in Figure 3C; 31% and 51%, respectively, in Figure 6). The remaining variance was evenly distributed among the remaining components, each contributing about 1% or less. When we performed the same analysis with data averaged across same-condition trials (thereby reducing the variation among vectors corresponding to the same concentration and odor pairs), the amount of variance accounted for by individual components greatly increased. For three-trial averages (across trials of the same concentration and odor), the first three and eight PCs (analyses similar to those in Figure 3C) captured 33% and 55% of the variance, respectively; with four-trial averages, these numbers were 37% and 62%, respectively. In both cases, the clustering of vectors within concentration clusters and the clustering of concentration clusters within odor superclusters was tighter, and the classification success was greater than with single-trial responses. Thus, the large variance unaccounted for by the first few PCs in the single-trial analyses is due to (small but widespread in dimension) variation across trials

and is unrelated to differences in the concentration or the identity of the stimulus presented.

Hierarchical clustering shown was performed using eight PCs and average linkage. Results were similar for nearest and complete linkages. The *k-means* method was also used for confirmation of clustering and showed similar results.

Two simple tests were used for classification, both based on Euclidean distances of individual points from group centroids (means of the remaining points in a group). In test A, points were individually classified as belonging to one of 15 (five concentrations of three odors) groups. Test A measures mainly trial-to-trial reliability. In test B, all points belonging to a particular concentration of an odor were taken out so as not to bias the location of group centroids and were then each classified as individually belonging to one of three (odor) groups. Test B measures similarity between concentration subclusters within an odor group. Results with other classification procedures, such as linear discriminant analysis, produced similar results. Classification results were also robust to the number of PCs used (from three upwards).

To bin PN spike times by oscillation cycle, cycles were identified using successive peaks of the band-pass-filtered (10–30 Hz) LFP. Spike counts were then computed for each so-defined cycle (bin). This analysis was performed only for those experiments in which high-quality LFP recordings could be obtained.

Distance and correlation matrices were computed by measuring pairwise distances and cross-correlations between all time slices (from stimulus onset to 1 s after the end of stimulus) across concentrations and odors. The distance and correlation matrices shown are for 50 ms time slice widths averaged over three trials. The t statistic was used to assess statistical significance for the correlation matrices (only statistically significant correlations with $p < 0.001$ are shown).

For nonlinear dimensionality reduction with locally linear embedding (Roweis and Saul, 2000), we used code from Sam Roweis (http://www.cs.toronto.edu/~roweis/lle/), with Gerard Sleijpen's code for the JDQR eigensolver (http://www.math.uu.nl/people/vorst/JDQR.html). In the figures shown for nonlinear dimensionality reduction with LLE, we used as input 110-D time slices, each 100 ms wide and averaged over three trials. Results obtained with slice widths of 50 ms are included as Supplemental Data (see Figure S5 at http://www.neuron.org/cgi/content/full/39/6/991/DC1). For a particular choice of embedding dimension, LLE requires only one user-specified parameter (K), the number of nearest neighbors to consider in the reconstructions of individual high-dimensional points. We chose values for K such that distances to the K nearest neighbors were, for all points, small (see Supplemental Figure S6). The results we obtained were qualitatively similar (i.e., concentration trajectories localized within odor manifolds) with a wide range of K values (8 to 25).

For the analysis of classification success using subsets of PNs, 5 to 100 PNs (in increments of 5) were randomly selected (100 combinations per number of PNs) from the pool of 110 PNs, and PCA was performed on each selection.

Acknowledgments

This work was supported by grants from the National Institute for Deafness and Communication Disorders, the National Science Foundation (BITS Program), the Keck and McKnight Foundations (to G.L.). M.S. received support from the Burroughs Wellcome Fund. V.J. was supported by the Sloan-Swartz Center for Theoretical Neurobiology at Caltech. We are grateful to Pietro Perona, Marzia Polito, Sam Roweis, Erik Winfree, Rainer Friedrich, and the Laurent lab for helpful discussions throughout the course of this work and for comments on the manuscript; to Ofer Mazor, Stijn Cassenaer, and Javier Perez-Orive for suggestions with the extracellular probe recordings; and to Sachiko Murase for vapor pressure calculations. Multichannel silicon probes were kindly provided by the University of Michigan Center for Neural Communication Technology, sponsored by NIH NCRR grant P41RR09754.

Received: May 8, 2003
Revised: August 6, 2003
Accepted: August 12, 2003
Published: September 10, 2003

References

Adrian, E. (1942). Olfactory reactions in the brain of the hedgehog. J. Physiol. (Lond.) *100*, 459–473.

Bäcker, A. (2002). Pattern recognition in the olfactory system of the locust: priming, gain control and coding issues, Ph.D thesis, California Institute of Technology, Pasadena, California.

Burrows, M. (1996). The Neurobiology of an Insect Brain (New York: Oxford University Press).

Cang, J., and Isaacson, J.S. (2003). *In vivo* whole-cell recording of odor-evoked synaptic transmission in the rat olfactory bulb. J. Neurosci. *23*, 4108–4116.

Cinelli, A., Hamilton, K.A., and Kauer, J.S. (1995). Salamander olfactory bulb neuronal activity observed by video rate, voltage-sensitive dye imaging. III. Spatial and temporal properties of responses evoked by odorant stimulation. J. Neurophysiol. *73*, 2053–2071.

de Bruyne, M., Foster, K., and Carlson, J.R. (2001). Odor coding in the *Drosophila* antenna. Neuron *30*, 537–552.

Drake, K.L., Wise, K.D., Farraye, J., Anderson, D.J., and Bement, S.L. (1988). Performance of planar multisite microprobes in recording extra-cellular single-unit intracortical activity. IEEE Trans. Biomed. Engineer. *35*, 719–732.

Engen, T., and Pfaffmann, C. (1959). Absolute judgements of odor intensity. J. Exp. Psychol. *58*, 23–26.

Freeman, W.J. (1978). Spatial properties of an EEG event in the olfactory bulb and cortex. Electroencephalogr. Clin. Neurophysiol. *44*, 586–605.

Friedrich, R.W., and Korsching, S.I. (1997). Combinatorial and chemotopic odorant coding in the zebrafish olfactory bulb visualized by optical imaging. Neuron *18*, 737–752.

Friedrich, R.W., and Laurent, G. (2001). Dynamic optimization of odor representations by slow temporal patterning of mitral cell activity. Science *291*, 889–894.

Gray, C.M., and Skinner, J.E. (1988). Centrifugal regulation of neuronal activity in the olfactory bulb of the waking rabbit as revealed by reversible cryogenic blockade. Exp. Brain Res. *69*, 378–386.

Heisenberg, M. (2003). Mushroom body memoir: from maps to models. Nat. Rev. Neurosci. *4*, 266–275.

Heisenberg, M., Borst, A., Wagner, S., and Byers, D. (1985). Drosophila mushroom body mutants are deficient in olfactory learning. J. Neurogenet. *2*, 1–30.

Hopfield, J.J. (1995). Pattern recognition computation using action potential timing for stimulus representation. Nature *376*, 33–36.

Joerges, J., Kuttner, A., Galizia, C.G., and Menzel, R. (1997). Representations of odours and odour mixtures visualized in the honeybee brain. Nature *387*, 285–288.

Joliffe, I.T. (1986). Principal Component Analysis (New York: Springer-Verlag).

Kauer, J.S., and Moulton, D.G. (1974). Responses of olfactory bulb neurones to odour stimulation of small nasal areas in the salamander. J. Physiol. *243*, 717–737.

Laurent, G. (2002). Olfactory network dynamics and the coding of multidimensional signals. Nat. Rev. Neurosci. *3*, 884–895.

Laurent, G., and Davidowitz, H. (1994). Encoding of olfactory information with oscillating neural assemblies. Science *265*, 1872–1875.

Laurent, G., and Naraghi, M. (1994). Odorant-induced oscillations in the mushroom bodies of the locust. J. Neurosci. *14*, 2993–3004.

Laurent, G., Wehr, M., and Davidowitz, H. (1996). Odour encoding by temporal sequences of firing in oscillating neural assemblies. J. Neurosci. *16*, 3837–3847.

Laurent, G., Stopfer, M., Friedrich, R.W., Rabinovich, M.I., Volkovskii, A., and Abarbanel, H.D. (2001). Odor encoding as an active, dynamical process: experiments, computation, and theory. Annu. Rev. Neurosci. *24*, 263–297.

MacLeod, K., and Laurent, G. (1996). Distinct mechanisms for synchronization and temporal patterning of odor-encoding neural assemblies. Science *274*, 976–979.

MacLeod, K., Bäcker, A., and Laurent, G. (1998). Who reads temporal

information contained across synchronized and oscillatory spike trains? Nature *395*, 693–698.

Margrie, T.W., and Schaefer, A.T. (2003). Theta oscillation coupled spike latencies yield computational vigour in a mammalian sensory system. J. Physiol. *546*, 363–374.

Marin, E.C., Jefferis, G.S., Komiyama, T., Zhu, H., and Luo, L. (2002). Representation of the glomerular olfactory map in the *Drosophila* brain. Cell *109*, 243–255.

Meister, M., and Bonhoeffer, T. (2001). Tuning and topography in an odor map on the rat olfactory bulb. J. Neurosci. *21*, 1351–1360.

Meredith, M. (1986). Patterned response to odor in mammalian olfactory bulb: the influence of intensity. J. Neurophysiol. *56*, 572–597.

Ng, M., Roorda, R.D., Lima, S.Q., Zemelman, B.V., Morcillo, P., and Miesenbock, G. (2002). Transmission of olfactory information between three populations of neurons in the antennal lobe of the fly. Neuron *36*, 463–474.

Pelz, C., Gerber, B., and Menzel, R. (1997). Odorant intensity as a determinant for olfactory conditioning in honeybees: roles in discrimination, overshadowing and memory consolidation. J. Exp. Biol. *200*, 837–847.

Perez-Orive, J., Mazor, O., Turner, G.C., Cassenaer, S., Wilson, R.I., and Laurent, G. (2002). Oscillations and sparsening of odor representations in the mushroom body. Science *297*, 359–365.

Pouzat, C., Mazor, O., and Laurent, G. (2002). Using noise signature to optimize spike-sorting and to assess neuronal classification quality. J. Neurosci. Methods *122*, 43–57.

Rabinovich, M., Volkovskii, A., Lecanda, P., Huerta, R., Abarbanel, H.D., and Laurent, G. (2001). Dynamical encoding by networks of competing neuron groups: Winnerless competition. Phys. Rev. Lett. *87*, 068102.

Rodiek, R.W. (1998). The First Steps in Seeing (Sunderland, MA: Sinauer Associates, Inc.).

Roweis, S.T., and Saul, L.K. (2000). Nonlinear dimensionality reduction by locally linear embedding. Science *290*, 2323–2326.

Rubin, B.D., and Katz, L.C. (1999). Optical imaging of odorant representations in the mammalian olfactory bulb. Neuron *23*, 499–511.

Spors, H., and Grinvald, A. (2002). Spatio-temporal dynamics of odor representations in the mammalian olfactory bulb. Neuron *34*, 301–315.

Seung, H.S., and Lee, D.D. (2000). The manifold ways of perception. Science *290*, 2268–2269.

Slotnick, B.M., and Ptak, J.E. (1977). Olfactory intensity-difference thresholds in rats and humans. Physiol. Behav. *19*, 795–802.

Stewart, W.B., Kauer, J.S., and Shepherd, G.M. (1979). Functional organization of rat olfactory bulb analysed by the 2-deoxyglucose method. J. Comp. Neurol. *185*, 715–734.

Stopfer, M., and Laurent, G. (1999). Short-term memory in olfactory network dynamics. Nature *402*, 664–668.

Stopfer, M., Bhagavan, S., Smith, B.H., and Laurent, G. (1997). Impaired odour discrimination on desynchronization of odour-encoding neural assemblies. Nature *390*, 70–74.

Turk, M., and Pentland, A. (1991). Eigenfaces for recognition. J. Cogn. Neurosci. *3*, 71–86.

Wachowiak, M., Cohen, L.B., and Zochowski, M.R. (2002). Distributed and concentration-invariant spatial representations of odorants by receptor neuron input to the turtle olfactory bulb. J. Neurophysiol. *87*, 1035–1045.

Wang, J.W., Wong, A.M., Flores, J., Vosshall, L.B., and Axel, R. (2003). Two-photon calcium imaging reveals an odor-evoked map of activity in the fly brain. Cell *112*, 271–282.

Wehr, M., and Laurent, G. (1996). Odour encoding by temporal sequences of firing in oscillating neural assemblies. Nature *384*, 162–166.

Wellis, D.P., Scott, J.W., and Harrison, T.A. (1989). Discrimination among odorants by single neurons of the rat olfactory bulb. J. Neurophysiol. *61*, 1161–1177.

Wong, A.M., Wang, J.W., and Axel, R. (2002). Spatial representation of the glomerular map in the *Drosophila* protocerebrum. Cell *109*, 229–241.